Scholastic Seed Inc.

www.gjeis.com

global Journal of ENTERPRISE INFORMATION SYSTEM

# Deep Learning Techniques for Automatic Prediction of Deviation in Left Ventricular for Heart Failure in 2D Echocardiography

**– Jyoti Mishra***

*Department of Electronics and Communication, University of Allahabad, Prayagraj, India*

*jyoti_jk@alldunv.ac.in* *https://orcid.org/0000-0001-5146-6837*

**– Mahendra Tiwari**

*Department of Electronics and Communication, University of Allahabad, Prayagraj, India*

*mahendra@alldunv.ac.in* *https://orcid.org/0000-0002-4095-7988*

**ARTICLE HISTORY**

**Paper Nomenclature:** Empirical Research Paper (ERP)

**Paper Code:** GJEISV14I3JS2022ERP2

**Submission at Portal (www.gjeis.com):** 03-Jul-2022

**Manuscript Acknowledged:** 13-Jul-2022

**Originality Check:** 15-Jul-2022

**Originality Test (Plag) Ratio (Ouriginal):** 08%

**Author Revert with Rectified Copy:** 17-Jul-2022

**Peer Reviewers Comment (Open):** 25-Jul-2022

**Single Blind Reviewers Explanation:** 05-Aug 2022

**Double Blind Reviewers Interpretation:** 10-Aug-2022

**Triple Blind Reviewers Annotations:** 23-Aug-2022

**Author Update (w.r.t. correction, suggestion & observation):** 26-Aug-2022

**Camera-Ready-Copy:** 03-Sep-2022

**Editorial Board Excerpt & Citation:** 10-Sep-2022

**Published Online First:** 30-Sep-2022

**ABSTRACT**

**Purpose:** The purpose of this study is to developed a deep learning technique has can automatically Predict the Deviations in Left Ventricular for Heart Failure in 2D Echocardiography

**Methodology:** Video-based deep learning program for object identification by definite detectors relied on the slice and fuse scheme, Retinal-SliceNet, which employs an allied, sole network having end-to-end training that dividing the left ventricle by dual attention Network in the Revebration labeling is extricated by picture denoising that sifts the denoised picture whose attribute is removed by administering controlled program DCNN called EchoNet-Dynamic exceeding the execution of human masteries in the crucial assignment of dividing the left ventricle; this is aimed at echocardiogram videos wherein the aimed paradigm precisely divides left ventricle having a dice Similarity coefficient of 0.92

**Findings:** The proposed structure is examined using cardiac illness data, and then the examining and preparing data are compared, yielding better outcomes with a veracity of 98%. Regarding the left ventricle's ejection fraction, outcomes are additionally compared and contradicted having an average association coefficient of 0.83 and an absolute average error of 5.0% creating outliers (region below the curve), which are narrowly under the intraobserver border. In this context, regions for enhancement are proffered. This outcome exhibits that our system is effectual to presage cardiac arrest.

**Originality:** A novel Approach such as Dissection and Artifacts Disposal used to presage cardiac arrest. Additionally, Improved technique of the DCNN paradigm training are discussed .Fast Fourier transform with Deep Convoluted Neural Network (FFT-DCNN) used as a better approach to speed-up the Convolution in frequency domain.

**KEYWORDS** Cardiorespiratory | Convolutional Neural Networks | Deep Learning | Dissection | Echocardiography | Medical Imaging | Segmentation

***Corresponding Author** (Jyoti Et. Al)*

- Present Volume & Issue (Cycle): Volume 14 | Issue-3 | Jul-Sep 2022
- International Standard Serial Number: Online ISSN: 0975-1432 | Print ISSN: 0975-153X
- DOI (Crossref, USA) https://doi.org/10.18311/gjeis/2022
- Bibliographic database: OCLC Number (WorldCat): 988732114
- Impact Factor: 3.57 (2019-2020) & 1.0 (2020-2021) [CiteFactor]
- Editor-in-Chief: Dr. Subodh Kesharwani
- Frequency: Quarterly
- Published Since: 2009
- Research database: EBSCO https://www.ebsco.com
- Review Pedagogy: Single Blind Review/ Double Blind Review/ Triple Blind Review/ Open Review
- Copyright: ©2022 GJEIS and it's heirs
- Publishers: Scholastic Seed Inc. and KARAM Society
- Place: New Delhi, India.
- Repository (figshare): 704442/13

## Introduction

Illnesses are a serious menace to man's well-being. Men war resisting illnesses in their whole lifespan by surmounting certain illnesses or habituating to these illnesses. As per the World Health Organizations (Correa AG, etal.,2007), the major ten reasons for demise at the international level in 2020 includes ischemic cardiac illness, strke, persistent blockage lung illness, reduced breathing disorders, Alzheimer's illness and rest of the dementias, pulmonary cancer, diabetes mellitus, transport wounding, dysentery, and TB alongside cardiovascular illness remaining the major reason of demise. In former researh, Mathers (Kumar A, et at.,2016)found out that cardiorespiratory illness remains the dominant reason for demise. In 2004, about 30% of females expired due to cardiorespiratory illness. In 2018, the demise count out of the major ten reasons of demise encompassed 73.8% of the entire demises in the US. (Papolos, et al.,2016).

The ticker remains one among the principal body parts in the human anatomy; the ticker acts as a pump dispatching blood towards numerous body parts and sinews. The blood transports oxygen and the rest of the nutriments for the cellular metabolic process and withdraws the refuse evolving out of the metabolic process. This study concentrates on human evaluation of cardial activity that is to be mechanized and analyses the novel spirit of in-depth learning for cardiac illness

Cardial activity remains important for facilitating common blood circulation in the body. Cardial malfunction results in wheezing, exhaustion, workout adversity, hydropsy, and enhanced fatality threat. Deterioration of heart activity is called cardiomyopathy or cardiac fiasco that remains a major reason for medicaments in the US and also remains an international wellness problem. Specifically, the dimension of left ventricular ejection fraction (percentage of modification in the left ventricular end-systolic and end-diastolic volume) remains one among the chief vital measurement of cardial activity since this recognize sick persons who are qualified for survival extending therapeutics (Koh AS, et al.,2017;Vos BD, et al., 2016b) . Nevertheless, the evaluation of ejection fraction consorted by substantial inter-onlooker capriciousness accompanied by inter-procedure disharmony relied on approach and process (Mathers CD, et al., 2009; Baumgartner CF, et al. (2017). (Shakir DK, & Rausl K.I, 2009; Ouyang D, et al., 2020; Yang D, et al., 2014; Folland ED et al.,1979). Left ventricular shape and activity are essential characteristics concerning sick-person administration, effect, and extended lifespan (Smistad E, & Lindseth F, 2014; Smistad E, et al., 2017). Hence, the examination of left ventricular volumes all through the cardial round alongside its allied indications emanated out of volume marks that is a usual duty in cardiology. Despite the fact that the American Society of Echocardiography and the European Association of Cardiovascular Imaging instructions suggest tracing alongside making on average of up to five succeeding cardial rounds when variability is noticed; the ejection fraction is frequently examined out of tracings of single indicative throb or visually estimated when the tracing considers being imprecise (Shakir DK, & Rausl K.I, 2009; Huang H,et al. 2017). It leads to elevated modification and restricted accuracy having inter-onlooker modification (Jaffer FA,et al., 2009, Carneiro G, et al. 2012; Cole GD, et al. 2015; Cole GD, et al. (2015); Litjens G, et al., 2017; Chen H, et al., 2015b; White HD, et al., 1987) measuring from 7.6% to 13.9%. Additional accurate assessment of cardial activity remains essential while sick persons have just a marginal decrease in ejection fraction that is exhibited for having substantially enhanced illness and fatality (Huang H, et al. (2017); Noble JA, & Boukerroui D (2006); Kips JG,et.al. (2008)). Aiming to administer medical reality, either required or information option is executed. Accordingly, a) a few patients are arduous to track, b) the dataset includes an extensive capriciousness of learning background, c) for a few sick-persons, segments of the wall are not observable in the pictures, d) for a few patients, the probe positioning suggestion for obtaining an arduous four-chambers outlook is plainly unattainable to stick to, and five-chambers outlook is obtained as an alternative. It creates an extremely heterogeneous dataset, concerning picture attributes and medical patients,that is normal medical execution information. Finally, many imaging procedures like echocardiography, cardiovascular magnetic resonance (CMR), cardiac computed tomography (CT), or positron emission computer tomography (PET). Pathological optical microscopy acts a vital part in finding out the structural and operative data of various body parts for identification and exploration.

Many types of approaches are employed for reckoning heart activity and identifying malfunction (Shakir DK, & Rausl K.I, 2009.)Subsequently, advanced mercantile results in LV division that yet need few levels of clientele association in both preparation phase and post division/tracing phase if rectification is needed Ouyang D, et al, 2020. Hence, the advancement of completely automated and quick approaches for LV volumetric analysis is needed.

## Contributions of the workflow:

Despite various results presently remaining for determining the item and dividing the LV; the absence of a general dataset of records causes it arduous for assessing and comparing their execution. Ensuing are the novel notions presented in this study:

- presents a general group of CAMUS (Cardiac Acquisitions for Multi-structure Ultrasound Segmentation) database. This consists of 2D echocardiographic series having twain or tetrad chamber outlooks of five hundred sick persons, which were obtained having the similar apparatus in a similar hospital. CAMUS contains physical mastery explanations for the left ventricle endocardium ($LV_{Endo}$), myocardium (epicardium contour, most precisely called LVEpi), and left atrium (LA).

- contributes an objection identification structure for continuously identifying the pictures in complete automated methodologies for the depiction of the LV boundary out of CAMUS at end-diastolic and end-systolic stages. The object identification is determined by the Retinal Slice Net the sliced images are segmented by attention network LU-Net-m15.
- compares advanced dissection programs in the area of ultrasonography cardiac picturing ensuing the abovementioned structure,
- Ascertaining and positioning every methodology in the segmented areas having the greatest faults; these faults owe to categorizing the LV for the ejection fraction and these Revebration artifacts in which these objects are pilfered by the denoising refiner, and this remains for contributing beneficial guidelines for additional examinations. The perfectly denoised pictures are prepared by the directed deep-learning program for discerning the cardiac aberrations. The Ejection fraction is calculated from the segmented bounding box and the reverberation artifacts are removed by the multiplane adaptive filter.
- The denoised segmented images are trained by the supervised DCNN to determine the outliers to formulate the area under the curve.

This study is structured as follows: Segment II reviews former studies on LV identification in CAMUS imaging, Segment III exhibits the assessment structure, Section IV presents a concise explanation of the 9 assessed methodologies, Sections V and VI discuss the outcomes of the engaged methodologies that are created by the online scheme, and, lastly, Section VII puts forth the conclusive comments and analysis.

## Former Studies

### 2D Object Identification:

Prevailing 2D object identifiers could be classified into one-phase and two-phase identifiers. One-phase item identification methods employ a solitary network for assessing the bounding box positions and category labels for a secured group of area propositions on the input picture. YOLO Pellikka PA, et al. (2018) separates an input picture into matrix flakes and employs an allied intricate network for reverting bounding boxes and class possibilities for every matrix flake. For dealing with items of dissimilar measures, SSDKips JG, et. al. (2008) presents characteristic pyramids along with anchor boxes of dissimilar feature proportions and measures for every characteristic map position Noble JA,& Boukerroui D (2006), suggests RetinaNet, which employs focal loss for dealing with the acute disparity betwixt the backdrop and intended item bounding boxes that cause the advanced identifying execution in item identification. Two-stage approaches initially create a tiny group of candidate areas and, ensuingly, purify the class labels alongside positions of these areas. The greatest indicative two-stage item identification program remains the R-CNN family of approaches [Smistad E, & Lindseth F (2014); Quien MM,& Saric M (2018); Smistad E, et.al.(2017)]. Based on it, the Faster RCNN scheme suggested by Quien MM, & Saric M (2018) puts forth the notion of an area proposition network for refining an enormous quantity of backdrop candidates; this is later employed as a secondary network for precisely prognosticating category labels and coordinates for every proposition. The studyby Huang H, et al. (2017). enhances identification precision additionally by presenting multiresolution characteristic pyramids into Faster R-CNN.

Various enquiries of echocardiographic dissection methodologies are suggested in 2D Chioncel, O, et al. (2017). Many of the mentioned methodologies concentrate on the dissection of the LVEndo border. Amidst these reports, Berard et al. (2016) that is issued in alone evaluated various approaches on a similar info-set. In this work, the writers enumerated the outcomes acquired by 9 various approaches. The mentioned methodologies could be separated into twain main classifications: the ones having a frail prior and the ones having a robust prior.

Heretofore, the area of bodily dissection was overwhelmed by atlas-based approaches (for instance, Xu JQ,et.al.(2020)) that possess the benefits of presenting robust dimensional priors and giving sturdy outcomes having reasonably less preparing information.

Anatomical object localization (in expanse or period), like body parts or markers, is a crucial pre-preparing phase in dissection works or the medical system for treatment arrangement and intercession. Localization in clinical imaging frequently needs analyzing of 3D volumes. For resolving 3D information by analyzing with deep learning programs, many techniques are suggested for handling the 3D expanse as a configuration of 2D quadrilateral levels. Yang et al., (2015) highlights markers on the farthest femur plane by preparing triad separate groups of 2D MRI slices (a slice per plane) with common CNNs. The 3D location of the marker is described as the junction of the triad 2D slices having the greatest categorization output.

Vos et al. (2016b) headed a phase additionally on localized regions of interest (ROIs) throughout bodily areas (tinker, aortic arch, and declining aorta) by detecting a rectangular 3D bounding box post 2D analyzing the 3D CT volume. Pre-prepared CNN structures, alongside RBM, are employed for a similar objective (Cai et al., 2016b; Chen et al., 2015b; Kumar et al. 2016) for surmounting the absence of information for studying finer characteristic representations. These researches show the localization work as a categorization work, and these common deep learning structures and studying procedures could be utilized.

The availability of additional information alongside the latest improvements in machine learning and parallel calculating structure and dissection approaches relied upon deep convolutional neural networks (CNN) have advanced like novel advanced techniques Ronneberger O, et al. (2015); Pellikka PA, et al. (2018).

Deep-learning methodologies are triumphantly inflicted on the dissection of the $LV_{Endo}$ in echocardiography. In 2012, Carneiro et al. created a two-phase deep learning methodology for the dissection of the $LV_{Endo}$ for 2D echocardiographic images limited to four-chamber overlook procurements Quien MM, & Saric M (2018). Relied on a maximal analytical structure, the writers have established the LV dissection issue as per twain consecutive phases: a) the automated choosing of various areas in the examined picture in which the LVEndo is completely available, b) the automated extrication of the LVEndo figure out of the former chosen areas. These twain phases encompass a deep brief network. This methodology was performed and developed on 400 pictures taken out of 12 various sick person series having many illnesses and examined on 50 pictures taken out of 2 fine and salubrious person series. The authors acquired a mean Hausdorff space of ~18 mm and an average mean complete space of ~8 mm for the $LV_{Endo.}$

In 2017, Smistad et al., exhibited the U-Net CNN methodology Norris R, et al., (1992), which can be prepared for triumphantly dissecting the left ventricle in 2D ultrasonography pictures. Nevertheless, because of the absence of preparing information, the network has been prepared and developed having the output of an advanced image distorted paradigm dissection methodology Leclerc S, et al. (2019). In the physically Segmented assessment group, the outputs display the acquirement of the similar precision having a Dice count of 0.87 by both the network and the distorted paradigm.

Lately, Oktay et al. (2021) utilized CNNs for dissecting the 3D LVEndo architecture employing a technique called anatomically constrained neural network (ACNN). The foundation of their neurological network relied upon a structure just like the 3D U-Net of Malm S, et al. (2004). which the dissection output is induced to suit a haphazard concise embodiment of the fundamental structure developed on the auto-encoder network. Execution of this methodology was examined on the CETUS info-set. Authors acquired the ensuing counts for the dissection of the 3D $LV_{Endo}$ architecture: a) mean Dice valuation of 0.912 (ED) and 0.873 (ES), b) mean Hausdorff spaces of 7.0 mm (ED) and 7.7 mm (ES), and c) average mean complete spaces of 1.9 mm (ED) and 2.1 mm (ES).

## Research Methodology

The below block diagram in Figure I represents the working structure of the proffered methodology. Initially, the input images have been trained from the input database, the training procedure has to undergo the preprocessing, object detection, segmentation, removal of artifacts, and training the segmented data to determine the heart abnormalities. In preprocessing, the image has been resized and the noise is removed initially, then the image has been cleaned. The removed noise has to undergo the augmented images for the large-scale training of the single frame and then the quality of the images is enhanced by the Contrast enhancement. The frequency component of the segmented images are the spatial and temporal convoluted images are then fused and sliced the detected images by the Retinal Slice Net, the sliced images are segmented by attention network LU-Net-m15, the Ejection fraction is calculated from the segmented bounding box and the reverberation artifacts are removed by the multiplane adaptive filter and then the denoised segmented images are trained by the supervised DCNN to determine the outliers to formulate the Area Under curve.

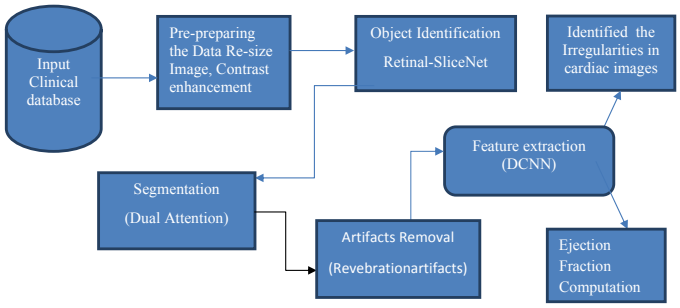


**Figure 1** Proffered framework of the detection of the heart abnormalities by Deep learning concepts

### Preprocessing

The unprocessed pictures gathered out of the scan institute and web pages are inappropriate for straight processing because of the presence of different noises in the pictures. Hence, it is required to preprocess this prior to the analysis. Preprocessing remains an essential phase that includes transformation, picture rescale, noise clearing, optimizing the standard, and creating a picture where trivial details could be ascertained perfectly.

### Picture Rescaling

Picture rescaling is a vital part of picture processing procedure for increasing and reducing the provided picture dimension in pel configuration. Picture interpolation could be split into twain various manners – picture down-sampling and upsampling that are required while rescaling the information for equalling neither the certain conversation medium nor the output display. As this is much suitable to transfer low-resolution variants to the client, an estimation of the initial high-resolution might be required for giving the last visual information. A precise rescaling of picture information is a vital phase in several implementations starting from many customer goods to crucial activities in the clinical, protection, and military divisions. This approach creates the last procedure quickly for processing the picture. Pace of rescaling could be computed by employing the process that affects out of the certainty that the consequential picture frequently has block artifacts that are not visibly distinct yet generally could extremely influence adversely too, and error computation is employed to relate the methodologies.

## Contrast Augmentation

For preparing the picture preferable for definitive implementations, contrast augmentation should be employed. This enhances the perceptibility and translucency of the picture, and the initial picture is agreeable to execute the computer.

When the picture values of the low contrast pictures are acute, the contrast augmentation extends the severity of pels. Generally, the picture could contain bad analytical degree or misstatement of pels neither because of less standard of the picturing instruments nor the acute outer surroundings amidst learning procedure. Amidst the several contrast augmentation approaches, histogram alteration process is widely employed due to its simplicity and efficacity. The procedure of histogram equalization acts to extend the severity of the input picture for producing a similar dispensation in order that the operational range of the picture is completely demoralized. Contrast remains the variation among maximal and minimal pel severity. Formula to extend the histogram of the picture to augment the contrast is

$$a(x,y) = \frac{b(x,y)-b_{min}}{b_{max}-b_{min}} * 2bpp \quad (1)$$

This formula needs to detect the minimal and maximal pel severity multiplied by degrees of gray. In our context, the picture is 8bpp, hence the degrees of gray are 256.

The minimal value remains 0 and the maximal value remains 225. Hence, the formula in our context is

$$a(x,y) = \frac{b(x,y)-0}{255-0} * 255 \quad (2)$$

in which f(x,y) represents the value of every pel severity. For every f(x,y) in a picture, we may compute this formula.

Subsequent to employing these equations, the capacity of the picture is enhanced. The chief aim of the contrast augmentation scheme is bipartite – domestically adaptable histogram equalization and decrease of unwanted items like noise and obstructing items.

## Assessment Framework

The slice-and-fuse technique influences 2D CNNs for hastening item identification and detection in HD thick 3D volumes. This technique depends on twain chief performances: the slice performance that efficiently encrypts 3D volumes into an accumulation of 2D pictures, and merge performance, which decrypts 2D prognoses for recuperating volumetrical assessment. Having these twain performances, the greatest arithmetically acute element called the learning-based expression for identification alongside dissection is exclusively conducted in the 2D expanse during which the remaining computing of the 3D information is arithmetically simple.

- **The slicing Performance**

Slicing creates a group of 2D slices for a solitary 3D volume. For creating an XY slice out of a thick 3D volume $V \in R\ Nx \times Ny \times Nz$, the sub-volume of dimension $Nx \times Ny \times n$ is trimmed initially, and later alike performances are implemented towards X and Y trajectories for acquiring an accumulation of XY and YZ slices. It creates a comprehensive $Nx/n + Ny/n + Nz/n$ 2D slices while the overlaying is absent betwixt twain slices in a single trajectory.

- **Computing every slice**

Every slice is later separately prepared and computed employing a 2D image-based CNN for acquiring 2D mark maps concerning item/dissection labels. When the prognoses at every slice are acquired, the fusing performer is administered for creating a 3D volume. Consider that 2D picture-based CNN remains the exclusive element, which requires for preparing the suggested scheme, that remarkably lessens arithmetical and retention load. During the preparing phase, 2D slices alongside their labels by slicing the solidity volumes and congruous ground-truth volumes.

- **The fusing performance**

For totaling XY, YZ, AND XZ slices prognoses, the slices out of a similar trajectory are directly incorporated for acquiring a volumetric prognosis for every trajectory. Particularly, for XY trajectory, Nz/n XY slices are directly incorporated synchronously with the z-axis for creating a 3D prognosis $\widehat{V}_{XY} \in \mathbb{R}^{N_x \times N_y \times N_z}$.. Likewise, $Vb_{YZ}$ and $Vb_{XZ}$ are created for YZ and XZ trajectories. For merging the multi-view 3D prognoses, the k biggest values are made a mean value out of triad trajectories voxel by voxel in which k represents the hyperparameter for various categories. Post the merging performance, a rough 3D voxel-labeling is acquired for every volume.

Retinal-SliceNet is chosen out of the RetinaNet structure Noble JA, & Boukerroui D (2006), employs a solitary network for reverting intended items' positions. As portrayed in figure II, post the creation of XY, YZ, and XZ slices out of an input 3D volume, every slice is computed separately employing a RetinaNet, which prognosis bounding boxes alongside their congruent certitude marks. Every 2D prognosis could be decrypted into unceasing count maps in which the bounding box areas are packed with value of congruent marks. Post acquiring entire 2D count maps out of triad trajectories, these are fed towards the fuse performance for obtaining a solitary 3D volumetric assessment that is additionally thresholded for remaining the concluding 3D evaluation.

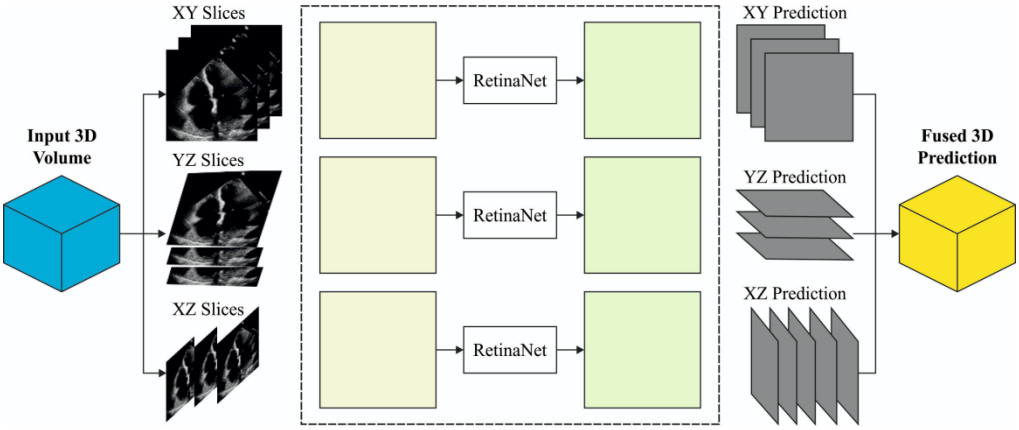


**Figure 2** SliceNet structures

Retinal-SliceNet is one-stage 3D item identification. This embodies RetinaNet Noble JA,& Boukerroui D (2006), into the slice-and-fuse structure for straight prognosticating the position of the intended items.

The next segment encapsulates an advanced method for picture dissection (SEG) that is relied on convolutional neural networks (CNNs). It has pictured in **figure 3** and the segmentation of the attenuated images.

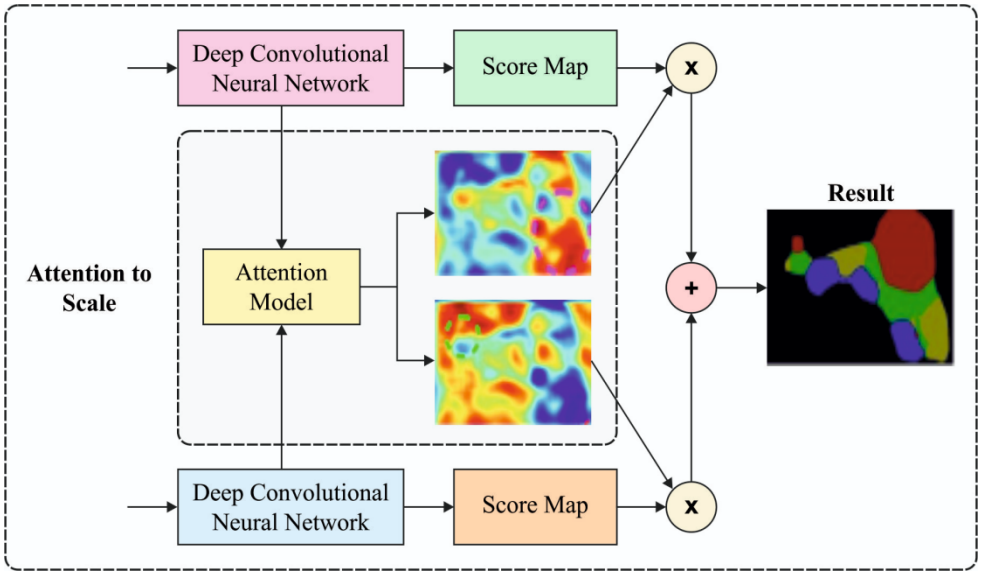


**Figure 3** Attention-based Semantic dissection paradigm

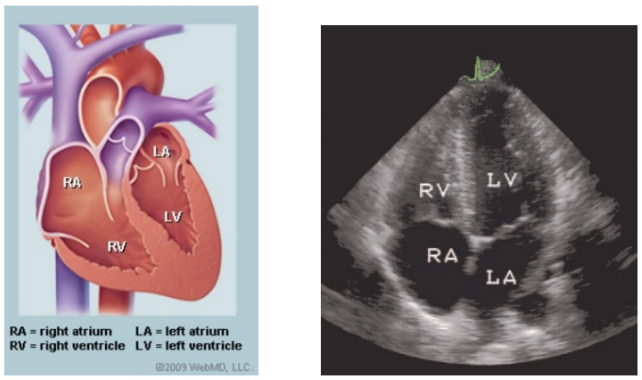


**Figure 4** The left picture depicts a traditional heart and the right picture depicts the Echocardiographic view (4C) of the heart

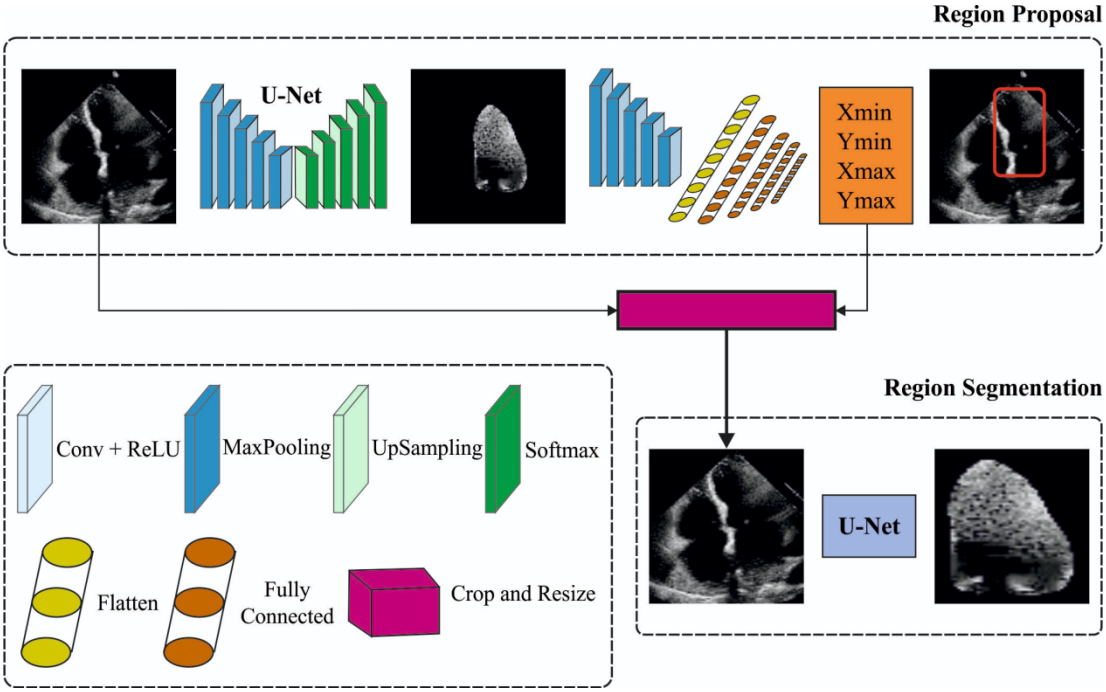


**Figure 5** Region Proposal Network (RPN) which scans boxes dispensed upon picture area and descries the ones which consist of items

**Figure 4** depicts the left picture of a traditional heart and the right picture depicts the Echocardiographic view (4C) of the heart. The multistep network is employed for enhancing the salubrity of dissection in 2D echocardiography. As the U-Net paradigm previously creates jazzed-up dissection outcomes in echocardiography Norris R, et.al. (1992), this structure is employed as the essence for the multistep network in this study, and it is called Localization U-Net (LU-Net). Lu-Net concentrates on positioning the LV prior to dissecting the endocardial and epicardial boundaries via an end-to-end learning process. Elementary supposition of the approach is that the combined processing of both these works must results in finer dissection outcomes. A portrayal of the LU-Net's comprehensive structure is presented in **Figure 5**. Specifically, LU-Net is comprised of twain chief components: an RPN for localization and a U-Net paradigm for dissection.

- **Scheme of U-Net Structure**

A similar U-Net structure is employed in the localization and dissection components. This comprises encryptor and decryptor phases, which possess many surfaces of 3x3 2D convolutional separator having ReLu initiation roles. During the encryptor phase, the merged picture out of the Retinal-SliceNet is prepared by an augmenting amount of separators accompanied by maxpooling subsampling post the convolutional surfaces. Arriving at a concluding spatial dimension of 8x8, the decryptor augments the spatial dimension steadily by upsampling and convolution phases having a dwindling amount of separators. Besides, the network possesses multi-skip circuits betwixt the encryptor and decryptor for recuperating the fine-grained spatial particulars, which can be missed post maxpooling. As the network was fashioned for contemporaneous executions, the amount of surfaces and convolutions are maintained to a minimum and employed 2D upsampling activities rather than exchanged convolution for decryptor. Outcome of this is a network having approximately 2,000,000 specifications that could dissect within milliseconds.

Network input is a solitary picture rescaled to 256x256 pels, and the output is a picture of a similar dimension as input having triad channels. Every channel is a regularized logit for every category by softmax initiation. Multilayer perceptrons (MLPs) are encompassed of tetrad corresponding coordinates of the BB (Bounding Box) throughout framework of focus, specifically, the amalgamation of the LV and myocardium, called ($x_{min}$, $x_{max}$, $y_{min}$, $y_{max}$). The MLP joined with the flattened output of the characteristic separator comprises of concealed surfaces of, accordingly, 1024, 256, and 32 unite together and a concluding surface of tetrad units devoid of initiation role for permitting reversion on the coordinates of the BB. Employment of a primary dissection, as medial characteristic maps, permits to get advantage out of the excellent comprehensive execution of the U-Net paradigm for controlling the reversion network. Additionally, as the U-Net paradigm that is employed is processed concerning the amount of specifications, the localization network gives the robust benefit to be simpler and quicker than many of the advanced techniques. When the referral BB is described as the minimum BBs alongside the epicardium boundary, the aimed coordinates are calculated having an extra margin m as

$$x_{\min}^{m} = x_{\min} - m * h, \quad x_{\max}^{m} = x_{\max} + m * h$$
$$y_{\min}^{m} = y_{\min} - m * w, \quad y_{\max}^{m} = y_{\max} + m * w \tag{3}$$

in which (ω, h) represent breadth and tallness of referral BB. Inducement to include boundary is for giving a few factors throughout the aimed framework for the dissection work.

- **Localization Network**

The proffered RPN encompasses an amalgamation of the U-Net paradigm whose framework is depicted previously, ensued by a typical reversion network. The reversion network has twain chief components: a) a characteristic separator similar to the downsampling component of the U-Net paradigm depicted previously that consists of 12 surfaces of 3x3 2D convolutional separators having ReLU initiation.

- **Dissection Network**

The output of the RPN is employed like a heed procedure for trimming and rescaling the input ultrasonography picture. The consequential picture is sent towards a secondary dissection network whose framework agrees with a U-Net paradigm. This is a beneficial one as this paradigm is presently the highest effectual one examined on the CAMUS info-set regarding a balance betwixt precision, pace, and dimension Norris R, et. al. (1992).

- **Concluding end-to-end technique out of Dissection**

For creating the complete network guidable end-to-end, trimming of input picture and rescaling of correlated ROI (red block in figure V) are fulfilled by bicubic interpolation employing exclusively dissimilar activities. Amidst the calculation of the dissection, losing happens in the secondary U-Net; this is required for trimming the real mask too in accordance with the anticipated BB (Bounding Box) so that similar areas are considered during the computation. It creates the secondary dissection losing activity to develop progressively during the preparing step. This phase is ascertained employing the similar bicubic dissimilar sampling technique as the one discussed atop. Both the U-Nets associated with this framework are definite networks whose heaviness is studied concurrently. Triad chief consecutive works are, hence, prepared at a similar period amidst the computing procedure: a) primary U-Net dissection is employed in the RPN, b) localization of the LV BB employing primary dissection, and c) concluding U-Net dissection executed on the ultrasonography picture trimmed employing the BB out of the localization network. Collectively, the various attributes depicted in this segment permit the gradients for streaming out of the output towards the input of the network. At the determination moment, relied on localization outputs, conclusive dissection outcome is later restored to initial coordinate workflow of the input picture.

- **Dice Similarity Coefficient (DSC)**

For calculating the precision of the automatic dissection program, confirmed information is needed. If this is acquired, the precision could be computed employing DSC. This is generally employed while assessing the execution of dissection methodologies. It calculates the spatial overlap betwixt medically illustrated reality and the automatic dissection in which the confirmed information and automatic dissection are binary pictures. The value for DSC lies betwixt 0 (nil overlap) and 1 (complete overlap). DSC is measured like in which A remains the automated dissected pels and B remains the medically illustrated pels (Babalola et al., 2008).

$$D = \frac{2|A \cap B|}{|A \cap B| + |A \cup B|} \tag{4}$$

- **Reverberation artifact**

The reverberation artifact contravenes the presumption that an echo comes back towards the transducer post a reflection. Hypothetically, if the ultrasonography wave is discharged out of the transducer, this communicates with the facade of the framework, and the mirrored wave is transferred straightly back towards the transducer creating a solo return cycle. In practice, the mirrored ultrasonography wave could experience a nearer reflector in its path back towards the transducer. A section of the wave journeys back towards the transducer as anticipated during which another section is alternately mirrored back towards the initial framework.

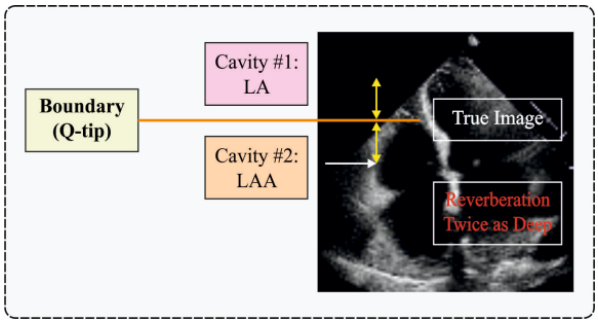


**Figure 6 Reverberation artifact in the left atrial appendage (white arrow) that may be conflated for a thrombus, where LA represents left atrium and LAA represents left atrial appendage.**

The section that is captured by the second reflector basically creates a second return travel by journeying back to the initial framework prior to creating this back to the transducer. Since the ultrasonography workflow presumes that the wave solely creates solo return travel, the transducer elucidates this lengthier trip period as a reflection approaching out of a framework that is farther than the initial framework. Hence, the transducer creates an artificial picture beneath the initial framework at double the space betwixt the transducer and the framework (**figure 6**). Coextending movement at this space could be generally viewed and remains a finer pointer of this artifact. The second reflector is frequently the transducer on its own, yet could also be other

general reflectors like the aorta, calcified framework, and infixed gadgets. Reverberation artifacts are prevalent in the rising aorta that is been viewed in 44%-55% of research and maintained to carry forth inconsistencies in the detection of disease and dispensable treatments. Uncomplicated reverberation artifacts are medically important too in detecting left atrial appendage thrombi (LAAT). Echocardiography is the methodology of selection for the investigation of LAAT. It is depicted in multitudinous clinical evaluation record that explains sick persons experiencing dispensable sternum surgeries owing to the misconception of aortic segmentation on echocardiography. These artifacts remarkably enhance inter-viewer capriciousness in the detection of LAAT. For reducing fiasco positive detection of LAAT, multiplane TEE (Transesophageal Echocardiography) must be employed alongside a methodical technique of picturing out of multitudinous windows and at a multitudinous angle Leclerc S, et al. (2019). Noise is filtered by the adjustment separator.

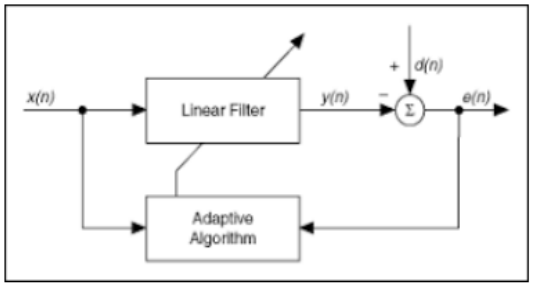


**Figure 7** Block illustration of General Adaptive Filter program having inputs and outputs

The adjustive adaptive program presents impulse reply of the separator and heavinesses are adapted by adaptable administration procedure is said pictorially in **Figure 7**. There are many programs attainable for extracting noise. Choosing a program relies on the kind of implementation that exhibits which kind of error indication is to be detached. The error indication is detached by employing LMS (Least Mean Square). This program modifies the separator heaviness vector valuation to such an extent that error signal e(nu) is diminished in an average square sense. The arithmetical portrayal of this program is given as Malm S, et. al. (2004).

$$\begin{aligned} y(n) &= w(n)*x(n) \\ e(n) &= d(n) - y(n) \\ w(n+1) &= w(n) + \mu * e(n) * x(n) \end{aligned} \quad (5)$$

## Training paradigm

In this segment, the facts regarding training and also the improved technique of the DCNN paradigm training are discussed is shown in architecture view in **Figure 8**. For enhancing the paradigm's universality competence, the input preparing specimens are unnaturally complicated employing frequency domain conversions that utilize the Segmented artifacts detached picture valuations. For the preparing paradigms, contrastingly, respiration movement artifacts detached betwixt the adjoining slices, which are recreated through in-lane rigid transitions that are specified for every slice individually. The correlated paradigms comprehend to an output having the temporal and spatial domain valuation. The Adam Optimization program (Machine Learning Mastery, Vermont Victoria, Australia) is employed for preparing. Post a hundred stages of preparing, the mean square error is computed for ascertaining the cardiac aberrations, and the cardiac fiasco is decided by frame to frame. A DCNN paradigm is prepared to possess remaining links and spatiotemporal convolutions through frames for prognosticating the ejection fraction. In contradiction of former CNN frameworks for machine learning of clinical pictures, this technique amalgamates spatial besides temporal data in the network convolutions. Spatiotemporal convolutions that integrate spatial data in bi-dimension in addition to the temporal data in the tri-dimension, which were formerly employed in non-clinical video-categorization works. Nevertheless, this technique is not formerly employed for clinical information provided the comparative insufficiency of specified clinical videos. Conclusively, video-level prognoses of the ejection fraction for throb-to-throb assessments of cardial activity are made. Due to the fact that the disparity in cardial activity could be made by modifications in uploading circumstances besides pulse rate in a category of cardial circumstances, it is suggested for executing evaluations of the ejection fraction for up till five cardial rounds.

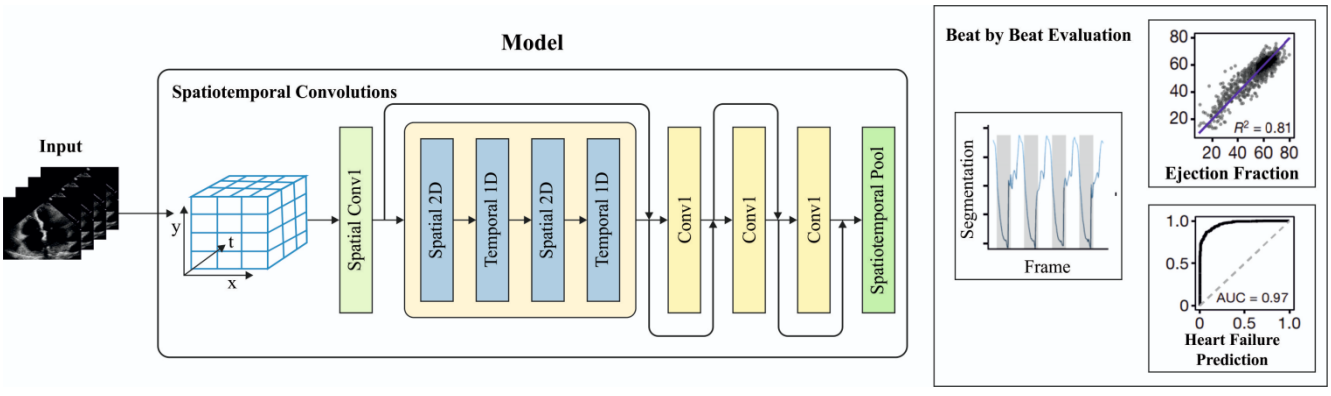


**Figure 8** Training Model for the detection of the Ejection Fraction of the Left Ventricular

### Enhancement practicing Fast Fourier transform with Deep Convoluted Neural Network (FFT-DCNN):

The Fast Fourier Transform (FFT) is an efficient technique to speed up the convolution. Conceptualization of applying Fourier domain DCNN operations approached to speed-up the Convolution in frequency domain. Normally, the image convoluted using spatial kernel functions has been converted using Fourier domain image, In this case, each convoluted pixel value is represented by a particular frequency restrained in the spatial domain image. The images are convoluted in the frequency domain with a significant speedup in training model time without reducing the system accuracy. Where FFT is an algorithm (i.e., a series of computations algorithm reduce the complexity of the convolution) is most significantly much more efficient Fourier transform algorithms

$$f[m,n] = \frac{1}{MN}\sum_{n=0}^{N-1}\sum_{k=0}^{M-1} F[k,l]e^{j2\pi\left\{\frac{mk}{M}+\frac{nl}{N}\right\}}[1] \quad (6)$$

where 0≤≤ m, k ≤≤M-1,0 ≤≤n,1 ≤≤N-1

Using FFT-DCNN images are convoluted in frequency domain to speed up the convolution and the pixel coordinates are represented by applying Fourier domain and the concept of Convolution is same as the context of conventional CNN techniques. The projected techniques limit the complexity raises with the benefit specifically in handling the larger images, and subsequently establish an expressive raise in network efficiency. The implicit notion of the Convolution theorem represents two functions $\kappa\kappa$ and u as shown in equation 7.

$$F(\kappa * u) = F(\kappa)\odot F(u)[2] \quad (7)$$

In the above equation F specifies the Fourier transform, * denotes convolution and $\odot\odot$ determines the Hadamard Pointwise product. The above equation is used to calculate Convolution more expeditiously using Fast Fourier Transforms (FFTs). Convoluting the pixel coordinates by applying Hadamard product in Fourier domain and it is determined by efficiency of the Fourier transform, the above technique concern significantly to minimize the computational operations than by utilizing sliding kernel frequency domain techniques, it performs much quicker than the spatial kernel function. Meanwhile, the Fourier domain is often applied in the platform of analyzing image processing, the concept of Fourier transform has been incorporated with the training model DCNN.

Below is the flow chart in **Figure 9** model for the proposed framed work model:

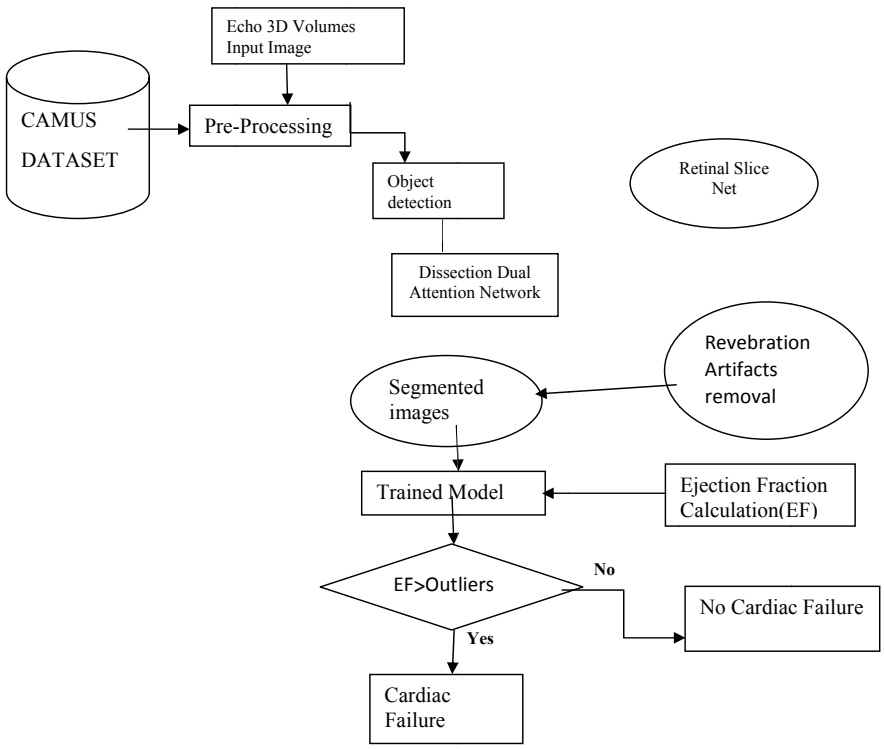


**Figure 9** Comprehensive flowchart of the suggested method

**Pseudocode to train the Segmented picture in the deep-learning model**

(i) Fix the Input: Input image $x_i$ out of the CAMUS Dataset

(ii) Estimated Output: Mean square error for ascertaining the AUC (outliers, Maximal count of Training epochs)

(iii) Ascertain intermediary outcomes, factors are intersection-over-union (IOU) metric, Bounding Boxes (BB)

(iv) Fix the context of the specifications enhanced to Adam Optimizer, connected with an ascertaining rate (either equal to 1e−3 or 1e−4) and a count of epochs (directed employing initial ceasing having the tolerance specification fixed set to 20), notice a sleek confluence of the preparing and confirmation depravations.

(v) Early fix the epochs as 100 for preparing the highlighted pictures.

**Stage 1**: The input pictures are downloaded from the CAMUS ECHOCARDIOGRAPHIC database and the input picture is loaded.

**Stage 2**: The input picture is sliced and merged by Retinal Slice net

**Stage 3**: The sliced merged 3D volumes of Echocadiography is split by employing the Localization and dissection network

**Stage 4**: The medical BB0ut is decided out of the sliced merged pictures by physical explanation.

**Stage 5**: The attention network is employed for ascertaining the dissection of the merged pictures.

**Stage 6**: The Revebration artifacts are detached by the multiplane and the adaptive separator.

**Stage 7**: The $LV_{EF}$ is decided by the $LV_{EDV}$ and $LV_{ESV}$ of Corr, Loe, and mae values physically.

**Stage 8**: The prognosis is decided by the outliers as the AUC

This is the pseudocode for the cardiac fiasco identification out of the suggested contributions, and this decides the cardiac fiasco out of the outliers.

# Results and Discussion

## Dataset Depiction

The database remained never suitable for learning the features of deep learning techniques, especially in 2D series. The information dispensed an anonymized array of 10,030 echocardiogram pictures that were employed for practicing echocardiography. Preprocessing of the pictures, containing anonymization and transformation out of DICOM form to AVI form videos, were executed alongside Open CV and pydicom.

Within this setting, the greatest universally obtainable and completely explained info-collection was presented to achieve 2D echocardiographic evaluation.

- **Dataset**

CAMUS data set included two- and four-chamber acquirements out of 500 sick people Norris R, et.at. (1992). The complete data-set was split into tenfold that was uniformly dispensed concerning image attribute (good, medium, and poor) and ejection fraction classification (≤45%, ≥55%, or in betwixt) of the ages of the sick people. It permited examination of complete info-dataset utilizing the traditional cross-confirmation technique. One cardiologist (O1) physically elucidated the endocardium and epicardium (LVEpi) boundaries of LV upon complete info-dataset at ED and ES and two other cardiologists (O2 and O3) upon a group of fifty sick persons. The group was already elucidated two times by O1 seven months apart. This process permited a correlation of the outcomes given by the programs having with the interobserver and intraobserver variabilities.

## Evaluation Metrics

- **Localization metrics**

The execution of the localization networks via intersection-over-union (IOU) metric and Manhattan space fiascos betwixt the anticipated and the cited BB coordinates (that is, its chief location (xc, yc), its height h, and width w). IOU remained traditional localization metric that calculated overlap betwixt anticipated BB and cited BB. This provided value betwixt 0 (nil overlap) and 1 (complete overlap). Besides, the 'BB out' metric was given which correlated to the number of cases in which anticipated BB did not comprehensively include cited mask listed in **Table 1.**

- **Segmentation metrics**

For calculating the precision of the dissection output ($LV_{Endo}$ and $LV_{Epi}$) of a provided methodology, Dice metric (associated nearby to the IOU and traditionally employed in dissection), mean absolute distance (dm), and the 2D Euclidian distance (de) were utilized. Dice likeness index was a standard of onlap betwixt user dissected surface Suser extricated out of a methodology and correlated reference surface Sref. This provided a value betwixt 0 (nil overlap) and 1 (complete overlap). dm correlated to mean space betwixt Suser and Sref, and at the same time, $d_e$ calculated the maximal local space betwixt the two layers. Furthermore, the attribute of dissection concerning cardiologists' explications was ascertained via the perception of outliers that were described as below.

**Table 1** - Location Precision of the existing and proffered techniques and evaluated alongside info-set of (500 sick persons).The error calculation

| Model | IOU | Error (mm) | | | | BB0ut |
|---|---|---|---|---|---|---|
| | | $X_c$ | $Y_c$ | H | W | |
| Faster R-CNN | 0.9099 | 1.3 | 1.3 | 2.9 | 2.8 | 1797 |
| AlexNet-m5 | 0.880 | 2.2 | 1.9 | 4.2 | 4.1 | 866 |
| VGG-m5 | 0.8880 | 1.9 | 1.7 | 4.0 | 4.0 | 903 |
| LU-Net-m15 | 0.9511 | **1.21** | **1.21** | **2.3** | **2.6** | 1801 |

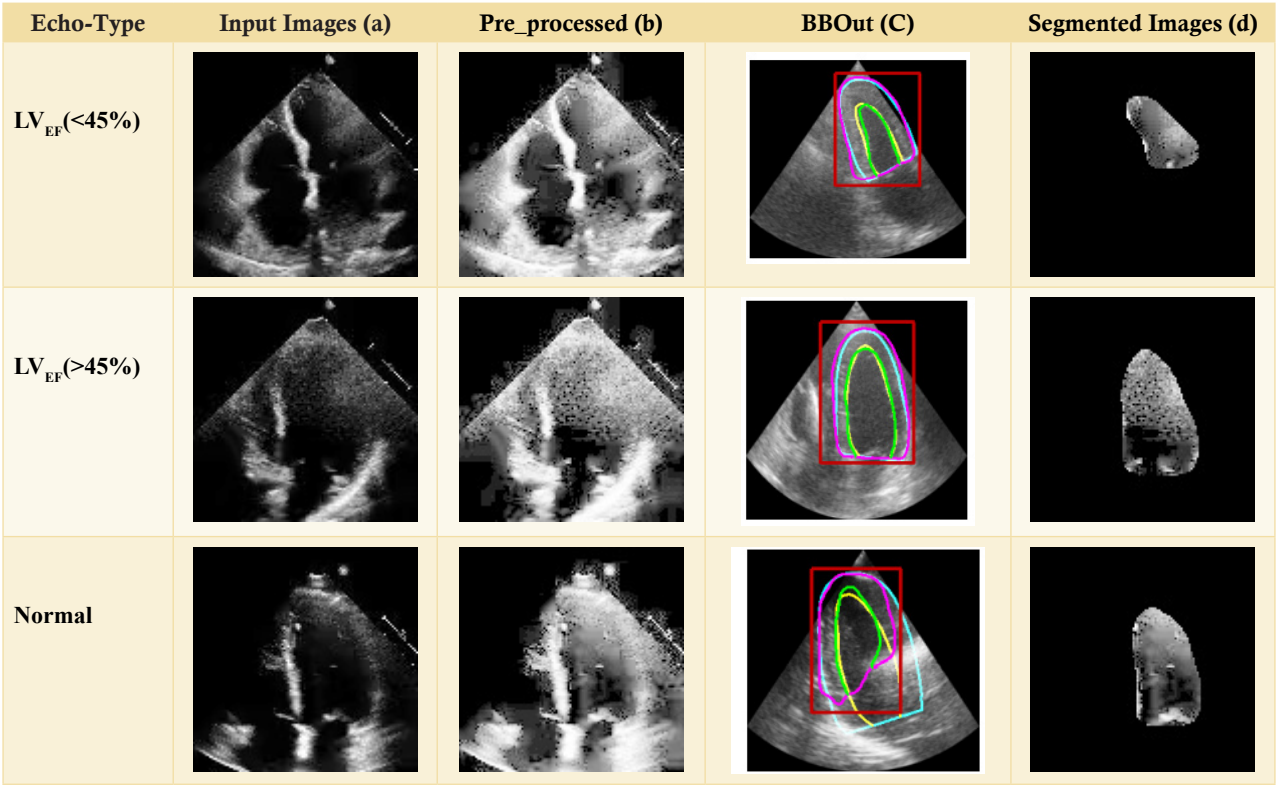


**Figure 10** Left Ventricular Ejection fraction for different values for the (a ) raw picture, ( b) pre-processed picture, (c ) Bounding Boxes (BB), (d) Segmented picture.

- **Medical metrics**

The execution of the methodologies with triad medical indices were assessed: a) the ED volume ($LV_{EDV}$ in ml), b) ES volume ($LV_{ESV}$ in ml), and c) ejection fraction (LVEF as a percent), wherein twain metrics were calculated – the Pearson correlation Co-efficient (corr), mean absolute error (mae), and the extremity of agreement (loa) (mean ± 1.96 std). Entire left ventricular volumes were calculated employing Simpson's biplane regulation https://www.who.int/news-room/fact-sheets/detail/the-top-10-causes-of-death including dissection outcomes on the two- and four-chamber apical outlooks tabulated in Table 2.

**Table 2** - Left Ventricular for EDV, ESV, and EF the existing and proposed techniques and evaluated with the data set of (500 patients).

| Model | $LV_{EDV}$ | | | $LV_{ESV}$ | | | $LV_{EF}$ | | |
|---|---|---|---|---|---|---|---|---|---|
| | Corr | Loa | Mae | Corr | Loa | Mae | Corr | Loa (%) | Mae (%) |
| Intra observer | 0.978 | -2.8 | 6.2 | 0.981 | -0.1 | 4.5 | 0.896 | -2.3 | 4.5 |
| U-Net1[36] | 0.947 | -8.3 | 10.9 | 0.955 | -4.9 | 8.2 | 0.791 | -0.5 | 5.6 |
| RU-Net[33] | 0.946 | -1.2 | 8.9 | 0.949 | 0.3 | 7.3 | 0.704 | -2.1 | 6.0 |
| AG-U-Net[34] | 0.956 | -1.4 | 8.1 | 0.962 | 0.6 | 6.2 | 0.798 | -2.2 | 5.5 |
| LU-Net-m15 | 0.952 | 2.4 | 8.1 | 0.962 | 1.8 | 6.5 | 0.821 | -1.2 | 5.0 |

- **Practicing metrics**

For calculating the precision of the dissection output ($LV_{Endo}$ and $LV_{Epi}$) of a provided methodology, Dice metric (associated nearby to IOU and traditionally employed in dissection), average absolute distance (dm), and Euclidian distance (de) were utilized. Dice likeness index was a standard of onlap betwixt the dissected surface Suser extricated out of a medical ejection methodology and the correlated reference surface Serf out of the practiced output AUC. This provided a value betwixt 0 (nil onlap) and 1 (complete onlap) having an IOU of 0.906 and (dc, yc, h, w) BB errors of (1.5, 1.5, 3.3, 3.5) mm, accordingly. Combining these outcomes gave the AUC (outlier) value that is tabulated in Table 3.

**Table 3** – Left Ventricular AUC for the existing and proposed techniques and evaluated with the data set of (500 patients).

| Model | $LV_{Endo}$ | | $LV_{Epi}$ | | AUC (outliers)% | | |
|---|---|---|---|---|---|---|---|
| | Dm (mm) | De (mm) | Dm (mm) | De (mm) | Anatoate (outlier) | Trained (outlier) | Mid_Both |
| U-Net1 (with artifacts removed) | 2.0 | 6.1 | 2.0 | 6.5 | 76 | 95 | 71 |
| LU-Net-m5 (with artifacts removed) | 2.1 | 7.0 | 1.9 | 6.2 | 80 | 88 | 85 |
| LUNet-m15 (with artifacts removed) | 1.8 | 5.7 | 1.6 | 5.3 | 91 | 96 | 97 |

The below figures 11 and 12 are practicing and validated precision for various Epochs values.

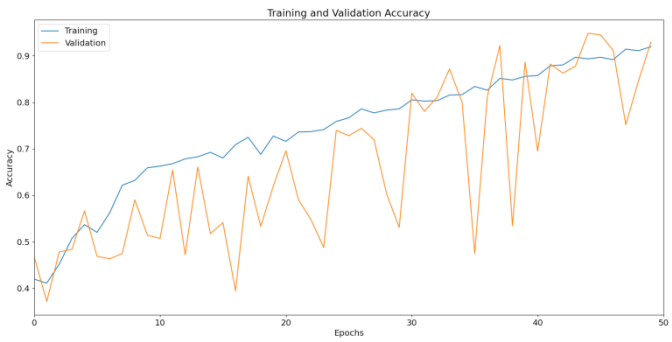


**Figure 11** Practicing and validated Accuracy for EF segmenting LU-Net Model

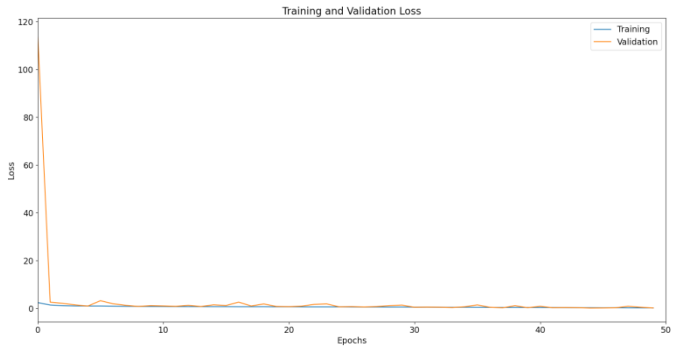


**Figure 12** Practicing and Validated Loss for EF segmenting LU-Net model

**Table 4** - Performance metrics calculation for the existing and proposed techniques and evaluated with the data set of (500 patients).

| Metrics | U-Net1 (with artifacts removed) | | LU-Net-m5 (with artifacts removed | | LU-Net-m15 (with artifacts removed | |
|---|---|---|---|---|---|---|
| | $LV_{Endo}$ | $LV_{Epi}$ | $LV_{Endo}$ | $LV_{Epi}$ | $LV_{Endo}$ | $LV_{Epi}$ |
| Loss | 0.282 | 0.263 | 0.317 | 0.273 | 0.274 | 0.258 |
| Pixel Accuracy | 0.965 | 0.973 | 0.968 | 0.975 | 0.975 | 0.977 |
| Dice score | 0.809 | 0.81 | 0.789 | 0.813 | 0.816 | 0.826 |
| IoU | 0.625 | 0.524 | 0.640 | 0.524 | **0.9511** | 0.9672 |

The above table gives the loss, pixel accuracy, Dice Score, and IoU values for the existing and the proposed techniques.

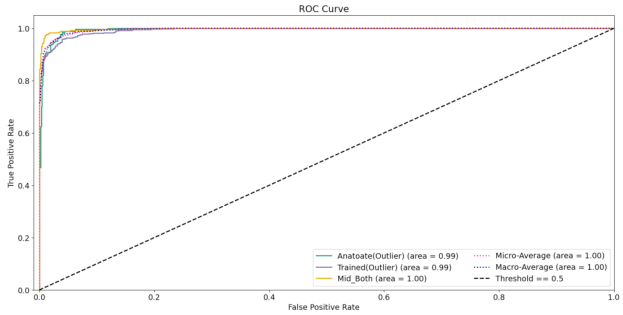


**Figure 13** ROC curve for the three classes of the 2D echocardiography

From the above Table 3, the ROC curve drawn in figure 13 for the three classes of the analysis of the Anatoate (outlier), Trained(Outlier), and Mid_Both.

## Conclusion

This study developed a slice-and-fuse technique that utilized 2D CNNs to trigger the Object identification in 2D echocardiography multiphase Attention networks to enhance the sturdiness of segmentation of left ventricular frameworks in 2D echocardiography. This network was assembled over the LU-Net structure and wascomprised of two phases: an RPN and a segmentation network. The Segmented areas had the greatest disasters wherein these disasters were because of specifying the LV for the fraction, and these artifacts were detached by the denoising separator, and this wasintended to give beneficial guidelines for additional explorations. The finely denoised images were trained by the well deep-learning techniques. The Segmented valuations were feature extracted, and it was trained by the Supervised techniques DCNN for ascertaining the cardiac aberrations. The execution of this result was evaluated on the present greatest open-access 2D echocardiographic info-set. This included 2D echocardiographic series having two- and four-chamber outlooks of five hundred sick persons, which were obtained with a similar apparatus in a similar hospital. CAMUS contained physical masterly explication for left ventricle endocardium ($LV_{Endo}$), myocardium (epicardium contour much precisely called $LV_{Epi}$), and left atrium (LA). a) An object detection ascertained by Retinal Slice-net for continually identifying the images following completely automated methodologies for the portrayal of the LV boundary out of CAMUS at end-diastolic and end-systolic steps; b) For localization, state-of-the-art segmentation using Attention network was employed, and it had been proposed. We demonstrated that employing an LU-Net to segment the heart followed by a BB regression network provided the optimum compromise for determining Ejection fraction accuracy and simplicity in the field of ultrasound cardiac imaging using the aforementioned framework. c) Identification and location of the segmented regions with the largest errors for each approach; these mistakes were due to the LV being labeled for the ejection fraction; these artifactswere detached by the denoising filter, and it was to provide beneficial recommendations for subsequent investigations. The supervised deep-learning technique was used to train the well-denoised images to detect heart abnormalities. Comprehensive segmentation scores were lesser than the intraobserver variability for the epicardial boundary having 11% of outliers, recreated nearby to the masterly examination for end-diastolic and end-systolic left ventricular volumes having an average association of 0.96, and enhanced evaluation of ejection fraction of LV containing scores that stays marginally greater than intraobserver's ones.

**Declaration of Conflict of Interest:** Authors declare that they have no conflicts of interest.

## References:


- Correa AG, etal. (2007) Artifact removal from EEG signals using adaptive filters in cascade. Journal of Physics: Conference Series**90** 012081.**doi:** 10.1088/1742-6596/90/1/012081
- Kumar A, Sridar P, Quinton A, Kumar RK, Feng D, Nanan R, Kim J (2016) Plane identification in fetal ultrasound images using saliency maps and convolutional neural networks. In Proc. IEEE International Symposium on Biomedical Imaging: 791–794. doi:10.1109/ISBI.2016.7493385.
- Papolos, Narula J, Bavish C, Chaudhry FA, Sengupta PP (2016) U.S. hospital use of echocardiography: insights from the nationwide inpatient sample. J. Am. Coll. Cardiol 67: 502–511.
- Koh AS, et al. (2017) A comprehensive population-based characterization of heart failure with mid-range ejection fraction. Eur. J. Heart Fail. 19: 1624–1634.
- Vos BD, Wolterink JM, de Jong PA, Viergever MA, Išgum, I (2016b) 2D image classification for 3D anatomy localization: employing deep convolutional neural networks. In Proc. SPIE on Medical Imaging: 97841Y. doi:10.1117/12.2216971.
- Mathers CD, Boerma T, Fat DM (2009) Global and regional causes of death. British Medical Bulletin 92(1): 7-32.
- Baumgartner CF, et al. (2017) An exploration of 2D and 3D deep learning techniques for cardiac MR image segmentation. International Workshop on Statistical Atlases and Computational Models of the Heart. Springer, Cham.
- Shakir DK, Rausl K.I (2009) Chemotherapy induced cardiomyopathy: pathogenesis, monitoring and management. Journal of Clinical Medicine Research 1: 8-12.
- Ouyang D, et al. (2020) Video-based AI for beat-to-beat assessment of cardiac function. Nature 580.7802: 252-256.
- Yang D, Zhang S, Yan Z, Tan C, Li K, Metaxas D (2014) Automated anatomical landmark detection on distal femur surface using convolutional neural network. In *Proc.* IEEE International Symposium on Biomedical Imaging: 17–21. doi:10.1109/isbi.2015.7163806.
- Folland ED, Parisi AF, Moynihan PF, Jones DR, Feldman CL, Tow DE (1979) Assessment of left ventricular ejection fraction and volumes by real-time, two-dimensional echocardiography. A comparison of cineangiographic and radionuclide techniques. Circulation 60(4): 760–766.
- Smistad E, Lindseth F (2014) Real-time tracking of the left ventricle in 3d ultrasound using kalman filter and mean value coordinates. In Proc. MICCAI Challenge on Echocardiographic

Three-Dimensional Ultrasound Segmentation (CETUS), Boston, MIDAS Journal: 65–72

- Smistad E, Østvik A, Haugen BO, Lovstakken L (2017) 2D left ventricle segmentation using deep learning. In Proc. 2017 IEEE International Ultrasonics Symposium (IUS): 1–4.
- Jaffer FA, Libby P, Weissleder R (2009) Optical and Multimodality Molecular Imaging: Insights Into Atherosclerosis [J]. Arteriosclerosis, Thrombosis, and Vascular Biology 29(7): 1017-1024.
- Carneiro G, Nascimento JC, Freitas A (2012) The Segmentation of the Left Ventricle of the Heart From Ultrasound Data Using Deep Learning Architectures and Derivative-Based Search Methods. IEEE Transactions on Image Processing 21(3): 968–982.
- Cole GD, et al. (2015) Defining the real-world reproducibility of visual grading of left ventricular function and visual estimation of left ventricular ejection fraction: impact of image quality, experience and accreditation. Int. J. Cardiovasc. Imaging 31: 1303–1314.
- Litjens G, Kooi T, Bejnordi BE, Setio AAA, Ciompi F, Ghafoorian M, van der Laak JAWM, van Ginneken B, S´anchez CI (2017) A Survey on Deep Learning in Medical Image Analysis. arXiv:1702.05747.
- Chen H, Ni D, Qin J, Li S, Yang X, Wang T, Heng PA (2015b) Standard plane localization in fetal ultrasound via domain transferred deep neural networks. IEEE J. Biomed. Health Inform. 19(5): 1627–1636. doi:10.1109/JBHI.2015.2425041.
- White HD, et al. (1987) Left ventricular end-systolic volume as the major determinant of survival after recovery from myocardial infarction. Circulation 76: 44–51.
- Huang H,et al. (2017) Accuracy of left ventricular ejection fraction by contemporary multiple gated acquisition scanning in patients with cancer: comparison with cardiovascular magnetic resonance. Journal of Cardiovascular Magnetic Resonance 19(1).
- Noble JA,& Boukerroui D (2006), Ultrasound image segmentation: a survey. IEEE Transactions on Medical Imaging 25(8): 987–1010.
- Kips JG, Segers P, Bortel LMV (2008) Identifying the vulnerable plaque: A review of invasive and non-invasive imaging modalities[J]. Artery Research 2(1): 21-34.
- Xu JQ, Murphy SL, Kochanek KD, Arias E (2020) Mortality in the United States, 2018. MD: National Center for Health Statistics, Hyattsville, Maryland, USA, NCHS Data Brief, no 355.
- Farsalinos KE, et al. (2015) Head-to-head comparison of global longitudinal strain measurements among nine different vendors: the EACVI/ASE Inter-Vendor Comparison Study. Journal of American Society of Echocardiography 28: 1171-1181.
- Leung K, Bosch J (2010) Automated border detection in three-dimensional echocardiography: Principles and promises. Eur. J. Echocardiogr. 11(2):97–108.
- Shah KS, et al. (2017) Heart failure with preserved, borderline, and reduced ejection fraction: 5-year outcomes. J. Am. Coll. Cardiol. 70: 2476–2486.
- Loehr LR, Rosamond WD, Chang PP, Folsom AR, Chambless LE (2008) Heart failure incidence and survival (from the Atherosclerosis Risk in Communities study). The American Journal of Cardiology 101:1016–1022.
- Bernard O, Bosch JG, Heyde B, Alessandrini M, Barbosa D, Camarasu-Pop S, Cervenansky F, Valette S, Mirea O, et al. (2016) Standardized Evaluation System for Left Ventricular Segmentation Algorithms in 3D Echocardiography. IEEE Transactions on Medical Imaging 35(4): 967–977.
- ic ek OC, Abdulkadir A, Lienkamp SS, Brox T, Ronneberger O 3D U-Net: Learning Dense Volumetric Segmentation from Sparse Annotation. In Proc. Medical Image Computing and Computer-Assisted Intervention – MICCA.
- Chioncel, O, et al. (2017) Epidemiology and one-year outcomes in patients with chronic heart failure and preserved, mid-range and reduced ejection fraction: an analysis of the ESC Heart Failure Long-Term Registry. Eur. J. Heart Fail. 19: 1574–1585.
- Oktay O, Ferrante E, Kamnitsas K, Heinrich M, Bai W, Caballero J, Cook SA, de Marvao A, Dawes T, O'Regan DP, Kainz B, Glocker B, Rueckert D (2018) Anatomically Constrained Neural Networks (ACNNs): Application to Cardiac Image Enhancement and Segmentation. IEEE Transactions on Medical Imaging 37(2): 384–395.
- Ronneberger O, Fischer P, Brox T (2015) U-Net: convolutional networks for biomedical image segmentation. In Navab N, Hornegger J, Wells WM, Frangi AF (eds) Medical Image Computing and Computer-Assisted Intervention – MICCAI 201. Springer Cham 9351: 234–241. Web. https://doi.org/10.1007/978-3-319-24574-4 2
- Pellikka PA, et al. (2018) Variability in ejection fraction measured by echocardiography, gated single-photon emission computed tomography, and cardiac magnetic resonance in patients with coronary artery disease and left ventricular dysfunction. JAMA Netw. Open 1, e181456.
- Quien MM,&Saric M (2018) Ultrasound imaging artifacts: How to recognize them and how to avoid them. Echocardiography 35(9): 1388-1401.
- Lang RM, et al. (2015)"Recommendations for cardiac chamber quantification by echocardiography in adults: an update from the American Society of Echocardiography and the European Association of Cardiovascular Imaging. Journal of American Society of Echocardiography16: 233–271.
- Norris R, White H, Cross D, Wild C, Whitlock R (1992) Prognosis after recovery from myocardial infarction: The relative importance of cardiac dilatation and coronary stenoses. Eur. Heart J.13: 1611–1618.
- Leclerc S, et al. (2019) Deep learning for segmentation using an open largescale dataset in 2D echocardiography. IEEE Trans. Med. Imag. 38(9): 2198–2210.
- Malm S, Frigstad S, Sagberg E, Larsson H, Skjaerpe T (2004) Accurate and reproducible measurement of left ventricular volume and ejection fraction by contrast echocardiography: comparison with magnetic resonance imaging. J. Am. Coll. Cardiol. 44: 1030–1035.
- The top 10 causes of death (2020) World Health Organization. Web. https://www.who.int/news-room/fact-sheets/detail/the-top-10-causes-of-death
- Bai W, Shi W, Ledig C, Rueckert D (2014) Multi-atlas segmentation with augmented features for cardiac MRI images. Medical Image Analysis 19(1): 98-109.
- Cai Y, Landis M, Laidley DT, Kornecki A, Lum A, Li S (2016b) Multi-modal vertebrae recognition using transformed deep convolution network. Comput. Med. Imaging Graph 51: 11–19. doi:10.1016/j.compmedimag.2016.02.002.
- Babalola, KO, Patenaude B, Aljabar P, Schnabel J, Kennedy D, Crum W, Smith S, Cootes TF, Jenkinson M, Rueckert D (2008) Comparison and evaluation of segmentation techniques for subcortical structures in brain MRI. In: Medical Image Computing and Computer Assisted Intervention–MICCAI 2008. Springer: 409–416.

**GJEIS Prevent Plagiarism in Publication**

The Editorial Board had used the Ouriginal – a Swedish anti-plagiarism software tool which is a fully-automatic machine learning text-recognition system made for detecting, preventing and handling plagiarism and trusted by thousands of institutions across worldwide. Ouriginal by Turnitin is an award-winning software that helps detect and prevent plagiarism regardless of language. Combining text-matching with writing-style analysis to promote academic integrity and prevent plagiarism, Ouriginal is simple, reliable and easy to use. Ouriginal was acquired by Turnitin in 2021. As part of a larger global organization GJEIS and Turnitin better equipped to anticipate the foster an environment of academic integrity for educators and students around the globe. Ouriginal is GDPR compliant with privacy by design and an uptime of 99.9% and have trust to be the partner in academic integrity (https://www.ouriginal.com/) tool to check the originality and further affixed the similarity index which is {8%} in this case (See below Annexure-I). Thus, the reviewers and editors are of view to find it suitable to publish in this Volume-14, Issue-3, Jul-Sep 2022.

## Annexure 14.12

| Submission Date | Submission Id | Word Count | Character Count |
|---|---|---|---|
| 03-Jul-2022 | D156209406 (Ouriginal) | 8804 | 60348 |

| Analyzed Document | Submitter email | Submitted by | Similarity |
|---|---|---|---|
| 1.2 ERP2_Jyoti_GJEIS Jul to Sep 2022.docx (D156209406) | jyoti_jk@allduniv.ac.in | Jyoti Mishra | 8% |

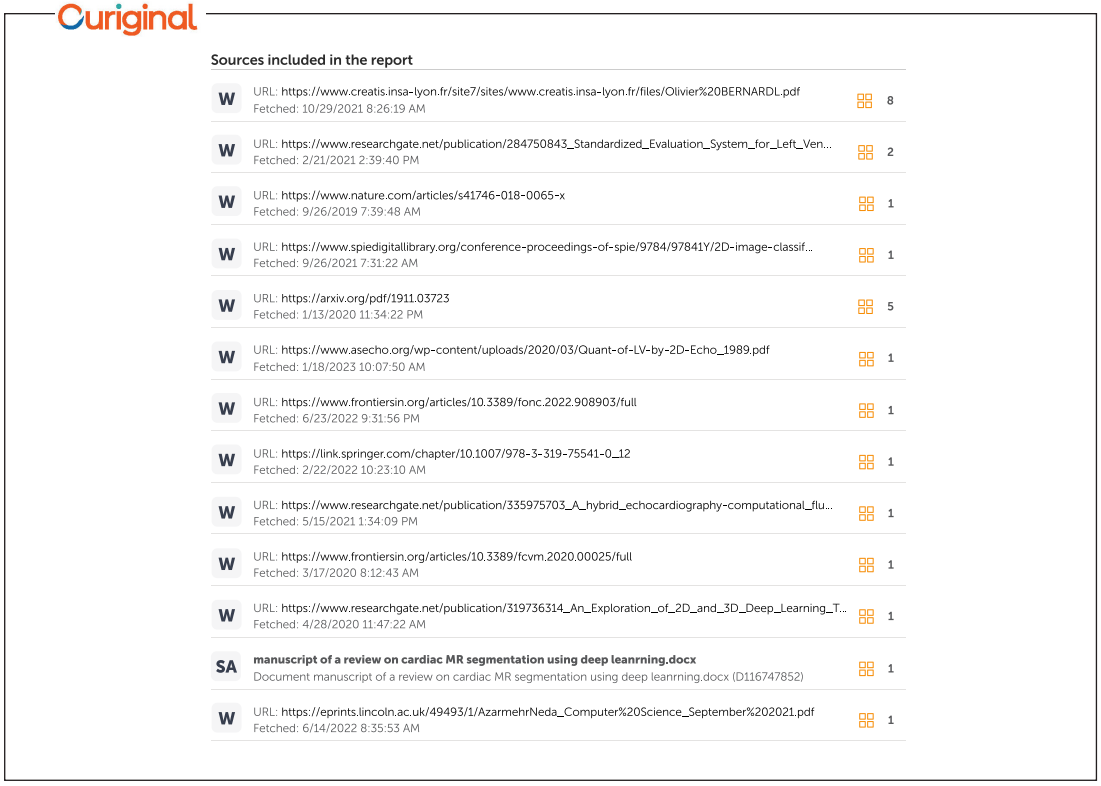

## Reviewers Memorandum

**Reviewer's Comment 1:** The title of the paper is quite significant and interesting. It talks about Deep Learning Techniques for Automatic Prediction of Deviation in Left Ventricular for Heart Failure in 2D Echocardiography.

**Reviewer's Comment 2:** Although the paper is technical in nature, it is very well structured and presented. Authors have made optimal use of graphs and figures to deliver the complicated thought in understandable and meaningful words.

**Reviewer's Comment 3:** This study is well structured and comprehensive. It reviews former studies on LV identification in CAMUS imaging, exhibits the assessment structure, presents a concise explanation of the 9 assessed methodologies, and discusses the outcomes of the engaged methodologies that are created by the online scheme, and, lastly, puts forth the conclusive comments and analysis.

**Citation**

Jyoti Mishra and Mahendra Tiwari "Deep Learning Techniques for Automatic Prediction of Deviation in Left Ventricular for Heart Failure in 2D Echocardiography" Volume-14, Issue-3, Jul-Sep 2022. (www.gjeis.com)

https://doi.org/10.18311/gjeis/2022
Volume-14, Issue-3, Jul-Sep 2022
**Online iSSN** : 0975-1432, **Print iSSN** : 0975-153X
**Frequency** : Quarterly, Published Since : 2009

**Google Citations:** Since 2009
**H-Index** = 96
**i10-Index:** 964

**Source:** https://scholar.google.co.in/citations?user=S47TtNkAAAAJ&hl=en

**Conflict of Interest:** Author of a Paper had no conflict neither financially nor academically.

## Editorial Excerpt

The article has 8% of plagiarism which is the accepted percentage as per the norms and standards of the journal for publication. As per the editorial board's observations and blind reviewers' remarks the paper had some minor revisions which were communicated on a timely basis to the authors (Jyoti & Mahendra), and accordingly, all the corrections had been incorporated as and when directed and required to do so. The comments related to this manuscript are noticeably related to the theme "**Deep Learning Techniques for Automatic Prediction of Deviation in Left Ventricular for Heart Failure in 2D Echocardiography**" both subject-wise and research-wise. Cardiac activity remains important for facilitating common blood circulation in the body. This study developed a slice-and-fuse technique that utilised 2D CNNs to trigger the Object identification in 2D echocardiography multiphase Attention networks to enhance the sturdiness of segmentation of left ventricular frameworks in 2D echocardiography. Overall, the paper promises to provide a strong base for further studies in the area. After comprehensive reviews and the editorial board's remarks, the manuscript has been categorized and decided to publish under the "**Empirical Research Paper**" category.

## Acknowledgement

The acknowledgment section is an essential part of all academic research papers. It provides appropriate recognition to all contributors for their hard work and effort taken while writing a paper. The data presented and analyzed in this paper by (Jyoti & Mahendra) were collected first handily and wherever it has been taken the proper acknowledgment and endorsement depicts. The authors are highly indebted to others who facilitated accomplishing the research. Last but not least, endorse all reviewers and editors of GJEIS in publishing in the present issue.

## Disclaimer

All views expressed in this paper are my/our own. Some of the content is taken from open-source websites & some are copyright free for the purpose of disseminating knowledge. Those some we/I had mentioned above in the references section and acknowledged/cited as when and where required. The author/s have cited their joint own work mostly, and tables/data from other referenced sources in this particular paper with the narrative & endorsement have been presented within quotes and reference at the bottom of the article accordingly & appropriately. Finally, some of the contents are taken or overlapped from open-source websites for knowledge purpose. Those some of i/we had mentioned above in the references section. On the other hand, opinions expressed in this paper are those of the author and do not reflect the views of the GJEIS. The authors have made every effort to ensure that the information in this paper is correct, any remaining errors and deficiencies are solely their responsibility.